Supporting Information - Born to be different: the formation process of Cu-nanoparticles tunes the size-trend of the activity for CO_2 to CH_4 conversion

Elena Gazzarrini,[†] Kevin Rossi,[‡,†] and Francesca Baletto[*,†]

[†]*Physics Department, King's College London, WC2R 2LS, London, UK*

[‡]*Laboratory of Computational Science and Modeling, Institute of materials, Ecole Polytechnique Fédérale de Lausanne, Lausanne, 1015, CH.*

E-mail: elena.gazzarrini@kcl.ac.uk

Phone: +39 351 5282408

I. Initial configurations

The structures employed in this study vary from a size of 110 to 976 atoms. The diameters range between values of 1.5 and 2.5 nm. We sequence the aGCN kind and occurrence in different structural motifs commonly observed in experiments. The geometries used are FCC structures, namely Octahedra (Oh) and their regular truncation (To), Icosahedra (Ih), marks-Decahedra (mDh) and defected Icosaheda resulting from a basin-hopping process (bh). The latter is obtained from an algorithm which allows to have transitions from a potential energy basin to another, by a canonical Monte Carlo simulation at constant T on the transformed cluster. In this framework, the transformation amounts to lowering the barriers between basins to the maximum possible extent, while keeping the levels of the minima unchanged.[1] The initial structures utilized for the CMD simulations are represented in Figure 1. The legend colors are an approximation to the nearest group (Ih, FCC or Dh) the clusters belong to.

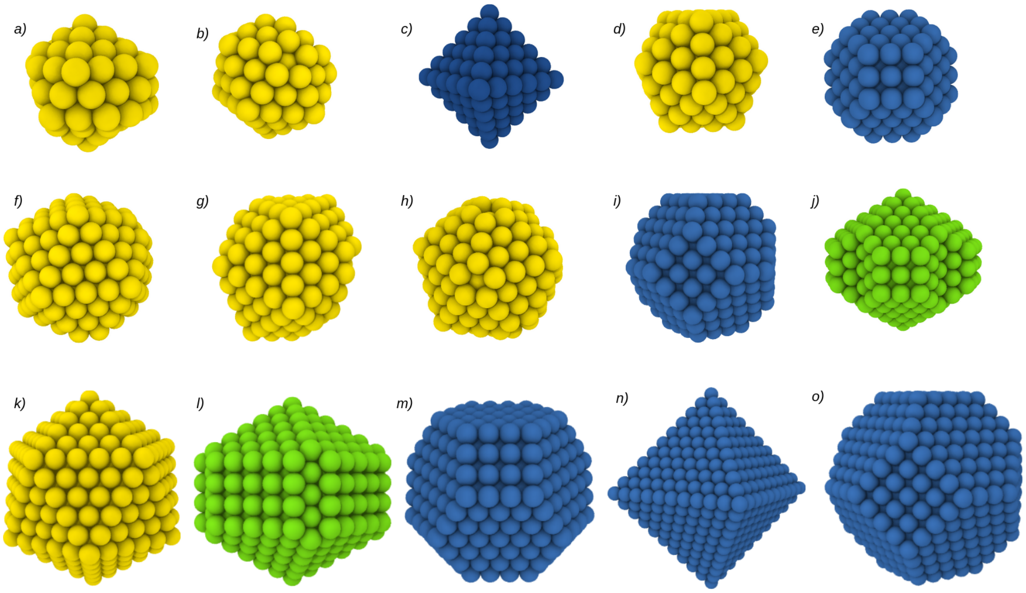

Figure 1: Initial structures for MD. *a*) Cu_{110} (bh), *b*) Cu_{130} (bh), *c*) Cu_{146} (Oh), *d*) Cu_{147} (Ih), *e*) Cu_{201} (To), *f*) Cu_{250} (bh), *g*) Cu_{270} (bh), *h*) Cu_{285} (bh), *i*) Cu_{405} (To), *j*) Cu_{434} (mDh), *k*) Cu_{561} (Ih), *l*) Cu_{585} (mDh), *m*) Cu_{586} (To), *n*) Cu_{891} (Oh), *o*) Cu_{976} (To). 🟨 is representative of Ih structures, 🟦 of FCC and 🟩 of Dh.

II. Classical Molecular Dynamics Simulations

Classical Molecular Dynamics is a computational algorithm which integrates Newton's equation of motion according to a finite difference method to simulate the time evolution of a system from certain initial conditions. A Velocity-Verlet algorithm[2] is exploited to evolve Newton's Equation of motion.

In this study, the software utilised to run MD simulations is LoDiS (Low Dimensional System), a FORTRAN90 computational engine specifically tailored to the study of processes at the nanoscale in finite-size systems. The LoDiS package allows different processes to take place, according to the initial parameters given.

In this study we investigate the freezing, the growth and the coalescence of Cu clusters. The atomic interaction is described by the RGL potential (Rosato-Guillope-Legrand potential[3]), which is dictated by the Equation 1:

$$E_i = \sum_{j \neq i}^{n} A e^{-p(\frac{r_{ij}}{r_0}-1)} - \sqrt{\sum_{j \neq i}^{n} \xi^2 e^{-2q(\frac{r_{ij}}{r_0}-1)}} \quad , \tag{1}$$

A and ξ are related to the cohesive energy, p and q tune the stickiness of the potential, while r_0 is the bulk nearest neighbor distance and r_{ij} is the set of all atomic coordinates. The parameters values for monoatomic Cu clusters are displayed in Table 1.

Table 1: Cu RGL potential parameters.

p	10.55
q	2.43
A[eV]	0.089
ξ [eV]	1.28
r_0 [Å]	2.56
E_{coh} [eV]	3.50

All the simulations are conducted with an Andersen thermostat which is used to mimic the interaction of the system with a heat bath. Its frequency is set at $5{\cdot}10^{11}$.

Annealing

Annealing (itMD - iterative Molecular Dynamics) processes are characterized by concatenated canonical NVT runs, where the temperature is lowered. The temperature is lowered by a factor of ΔT every time step $\Delta\tau$, resulting in a freezing rate of $\rho = \Delta T/\Delta\tau$.[4] The ratio ρ tunes the cooling/heating parameter which impacts the kinetics of the liquid-solid transitions. This process allows to get caloric curves, to determine freezing points and to investigate liquid-solid transitions kinetics. In this study the initial temperature is set to 1200 K. At this point the structure has already been melted with a fast (itMD) melting, so it lacks any geometry. The temperature is lowered by 25 K at every time step, until a minimum of 400 K. The freezing is conducted over a time of 160 ns at a rate of 5K/ns, corresponding to 1 million steps.

Growth

Atom by atom deposition happens on an initial metallic nucleus, thermalization and relaxation of the cluster are allowed between two depositions. This is a simulation where the temperature is fixed and on the original NP cluster, n atoms, one at the time, are deposited every τ steps and allowed to thermalize for 2τ steps. Atoms are shot towards the center of mass from a sphere 3 times larger of the NP with a velocity extracted from a Boltzmann Distribution coherent with the temperature of the source. Growth processes are run at a fixed NVT temperature of 600 K for 60000 steps for a total of 255 ns. Three initial structure are taken as the starting point: Cu_{146}, Cu_{147}, to which 850 atoms are added, and Cu_{201}, which receives 795 deposited atoms. This choice is motivated by the will to start from three different structures (a Decahedron, an Icosahedron and a FCC structure), and analyze how this factor influences the evolution of the system.

Coalescence

Coalescence is the process by which two clusters are brought into contact. Following thermalization, one of the clusters can be translated towards the other with kinetic energy comparable to the system's initial temperature. Once in contact, the clusters are left to evolve and aggregate under the potentials with a temperature lower than the initial one, tuned by the Anderson thermostat. The impact velocity plays a significant role in the formation process of the final aggregate. Whereas growth involves a step by step increase in total energy and atomic number allowing for thermalization between depositions, coalescence is an immediate process with an aggregation time shorter than the time scale to equilibrate. Coalescence processes are run for a shorter amount of time, since the focus is on the structural analysis at some specific time steps, namely when the two NPs are placed at a distance from each other, when they collide and when they merge together, forming one elungated structure. The simulations are started when the two NPs are at a distance of 6 nm along the z axis, and are run at a temperature of 600 K for 20000000 time steps, resulting in a total simulation time equivalent to 100 ns. The combinations are: Cu_{110}+Cu_{130}, Cu_{270}+Cu_{250}, Cu_{147}+Cu_{434}, Cu_{285}+Cu_{434} and Cu_{405}+Cu_{434}. These sizes are comparable to the ones employed in the previous processes, so that a full comparison between the three of them is achievable.

To the extent of gathering relevant statistics, four simulations are run for the same system. This is accomplished by exploiting Lyapunov instabilities, which state that atoms' trajectories are extremely sensitive to small differences in initial conditions. Changing the variable *irand* in the input file enables to generate different initial atomic velocities, and therefore to produce uncorrelated simulations.

III. Geometric Analysis

To determine NPs' geometries we adopt the common neighbor analysis (CNA). This is accomplished by examining the local connectivity of each pair of nearest neighbors. Each pair is associated a specific signature: (jkl), where j is the number of common nearest neighbors, calculated by looking at the first minimum of a pair distribution function, k is the number of bonds between the common nearest neighbors and l is the length of the longest chain between them.[5] The structures outputted from each different process are then categorised by looking at the CNA signatures of three main groups: FCC (Oh and To), Ih and Dh. Some examples of how to interpret the CNA pattern are:

1. a (555) signature characterizes a five-fold symmetry axis, and will be therefore abundant in an Ih structure. It will be in part present in a Dh NP as well, but should be absent in an ideal FCC.
2. (421) is the signature for an FCC environment, but it is always abundant in the bulk, and is therefore present in each structure.
3. a (422) symbolizes twinning planes and represents a grain boundary. It is therefore absent in an ideal FCC.
4. a (200) signature suggests the formation of square facets, and should be absent in an ideal Ih.
5. (100) is absent in an ideal Oh, but present in a To.
6. (111) and (311) signatures are representative of an FCC environment.

These rules are taken into account when categorizing the final structures resulting from the freezing, growth and coalescence processes in groups (FCC, Ih or Dh). The structures are considered defected (dFCC, dIh, dDh) when less than 70% of the CNA pattern is not in line with the expected group's ideal geometry.

IV. Setting the NanoCHE

The CHE approach pioneered by Norskov and co-workers represents a very promising way to enable modeling of electrochemistry by quantitatively incorporating insights from first-principles calculations.[6] The inclusion of quantum mechanical data imparts predictive capability and eliminates the need to make drastic simplifying assumption in the model. At the core of this approach is a specified reaction mechanism and the evaluation of the free energy of the corresponding elementary steps, $\Delta G = \Delta H - \Delta S$, where H is the enthalpy and S is the entropy of the reaction. The key gateway to introduce electronic structure information into the model is via the free energy of individual component in each of the elementary step.[7]

A linear scaling relationship between the binding energy and the aGCN for each step of the CO_2 reduction reaction is taken from the work by Zhao et al.[8] The relation seems particularly strong for the intermediates which bond with the active site through a carbon atom, such as CO^* and CHO^*.

The limiting potential U_L for a reaction step is defined as the difference between the free energies of the involved reactants, minus the chemical potential of a proton-electron pair calculated as half of the chemical potential of gas-phase H_2 at 0 V. U_L can be plotted as a function of the aGCN, as can be seen in.[8] The distances between the U_L=0 line and the most negative U_L line represent the minimum potentials required to guarantee all reaction steps to be exothermic. The three most negative U_L lines outline the so-called volcano plot. The intersection between the first and the second line at GCN = 3.1 defines the volcano top, which represents the lowest possible overpotential for $CO_2 \rightarrow CH_4$ on Cu surfaces. The equations which relate the limiting step reaction free energies ΔG to the aGCN are as follow:

$$\Delta G = \begin{cases} +0.162\, aGCN - 1.11, & \text{if } aGCN < 3.1 \\ -0.067\, aGCN - 0.416, & \text{if } 3.1 \leq aGCN < 8.4 \\ -0.222\, aGCN + 0.849, & \text{if } aGCN \geq 8.4 \end{cases} , \qquad (2)$$

where the first line corresponds to the reaction step $OH^* \xrightarrow{H^*} H_2O$, the second line to the reaction $CO^* \xrightarrow{H^*} CHO^*$, and the third to $CO_2 \xrightarrow{H^*} COOH^*$.

Once this relation is set up, the aim of this study is to calculate the current density, j, produced by each nanocluster. This is achieved through Equation 3.[6]

$$j_{NP}(t,T,U) = \sum_{i \in \{\mathrm{aGCN}\}} C \, \frac{\Omega(i)}{N_{sites}} \; i \; e^{\beta(\Delta G(i) - neU)} \qquad . \tag{3}$$

The current density measurement appears at a certain temperature T which determines the Maxwell-Boltzmann factor. {aGCN} refers to the aGCN fingerprint. Each aGCN fingerprint appears with a specific occurrence Ω, and N_{sites} corresponds to the number of surface sites for which the coordination number is calculated. The number of sites which participate in the reaction each time is defined by n, and is therefore equivalent to 1 since we are only considering atop sites; e is the electron charge and U is the applied potential, measured in eV/e. The pre-factor C is a constant fitted to reproduce the known specific current of low-Miller index surfaces and has units of mA/cm^2 .

It is therefore worthy to point out that various attempts were made to calculate the constant in Equation 3, which is eventually set equal to $-3.01 \cdot 10^{14}$ mA/cm^2. The most consistent method which leads to this value makes reference to the work by Loiudice et al.,[9] where the current density j produced by Cu nanocubes of different sizes is calculated. Since j is normalized in three different ways (geometric, electrochemical and nanocrystal area), the current density used is averaged over all the three normalisations. The 24 nm cube is chose due to its smaller size. It is known from[10] that large-sized cubes present 8 sites with aGCN equivalent to 2 (0.044% of sites in the case of a 24 nm cube) and 24 sites with an aGCN of 5.08 (0.131% of sites for a 24 nm cube). The rest of the composition for a 24 nm cube is; 2.498% of sites with an aGCN equal to 3.67, 4.865% with aGCN 5.83 and the majority of sites, 92.462%, presenting an aGCN signature of 6.67. The percentages corresponding to the aGCN of 3.67 and 5.83 scale linearly with the cube's size, while the higher aGCN composition increases quadratically with the NP's size. The current density - averaged across j_{geom} (-9.1 mA/cm^2), j_{ECSA} (-7.2 mA/cm^2) and j_{NC} (-5.7 mA/cm^2) - produced by such cube at an applied potential of -1.1 V in 0.1 M $KHCO_3$ and at room temperature is -7.33 mA/cm^2, where the glassy carbon background signal has already been subtracted.[9] The relation between the aGCN values and ΔG of Equation 2 is employed, and Equation 3 is reversed in order to find the constant C, at U=-1.1eV which results in a value of -3.01 $\cdot$ 10^{14} mA/cm^2.

V. Energetic Analysis

The shape of a nanocluster is strictly connected to its stability, since the binding energy is proportional to volume and surface parameters, with the two terms being in competition.[1]

Comparative energetic analysis of structural stability can be carried out by looking at the excess energy, ΔE, evolution. It is defined as the energy in excess with respect to having N atoms in the bulk, weighted by the number of atoms in the surface, as in Equation 4:

$$\Delta E = \frac{\mathrm{E_{coh}} - \mathrm{E_{pot}}}{\mathrm{N}^{2/3}} \qquad , \tag{4}$$

Where N is the number of atoms in the cluster, $\mathrm{E_{coh}}$ is the cohesive energy of the atoms in the bulk and $\mathrm{E_{pot}}$ is the potential energy of the relaxed nanocluster.

Since each simulation is run four times, the excess energy evolution through time of each of the four resulting structures is shown and discussed, and a brief analysis is performed to understand how different the features of each structure are. To get a physical result, the four excess energies are averaged into a $<\Delta E>$, which is also plotted against time for each process. The energy comparisons between freezing, growth and coalescence mainly come from this last characterisation.

The energetic behaviour of the NPs tells about the nature of the process: a structure which has a lower excess energy is more energetically favourable, and therefore more likely to be observed . Once all the processes are run, it is evident that more ordered structures (mainly ones resulting from a freezing process) are the most energetically favourable ones. We also note that the excess energy decreases monotonically with the NP's size.

Annealing

In Figure 2 we report the excess energy versus time/temperature for nanoparticles undergoing a phase change from the liquid to the solid phase. The inflection point in the energy function identifies a phase change: over a short time period, the excess energy is drastically lowered.

As a general trend, the structures which undergo a phase transition earlier are more likely to be more energetically favourable, leading to a more ordered structure.

Further we note a correlation between size and excess energy both for the case of liquid as well as solid structures.

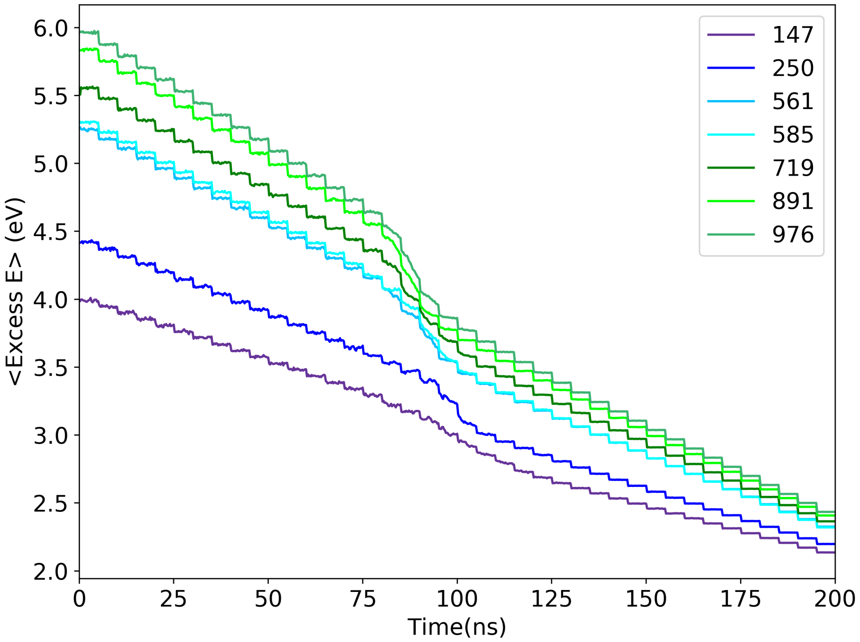

Figure 2: Excess energy development in freezing processes at a rate of 5 K/ns. The results are an average over the 10 independent runs for each size. The legend represents the number of atoms, namely the size of the NP.

Growth

Figure 3 shows the time/number of atoms evolution of the excess energy averaged over 10 independent atom-by-atom growth runs, for three different initial seeds.

Also in the case of atom-by-atom growth, the more ordered the structure, the lower its excess energy.

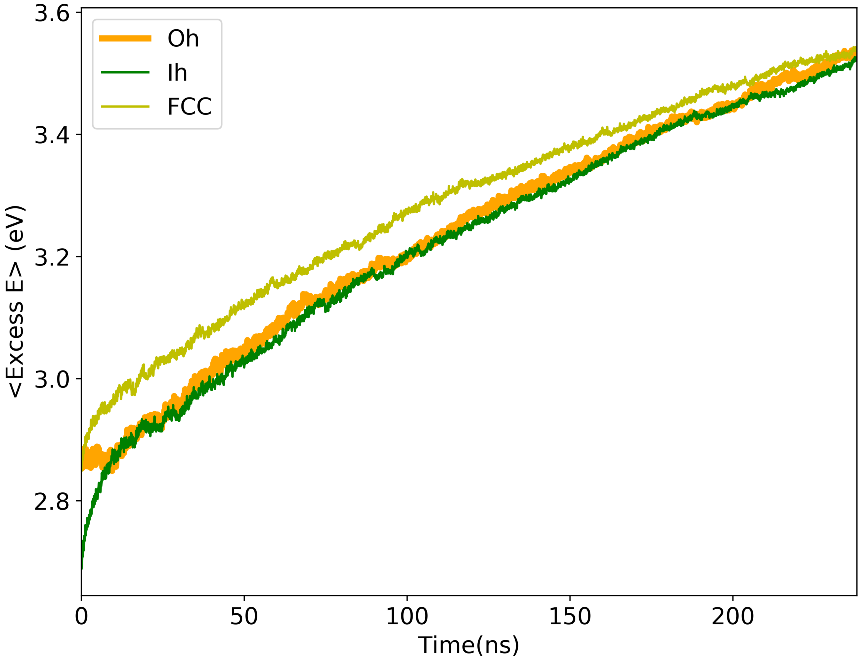

Figure 3: Excess energy evolution in growth processes. A Gaussian Kernel is applied to the averaged results to enhance readability. The legend represents the number of atoms, namely the size of the NP.

One may observe from Figure 3 that the Ih and Oh structures are the most energetically favourable throughout the whole size range. The FCC remains the least favourable one for the whole simulation.

Coalescence

Figure 4 depicts the excess energy evolution in the coalescence simulations performed. All the structures have a maximum in excess energy at the beginning of the simulation, when they are far apart one another.

There is a proportional increase in excess energy with the size of the collided cluster. The Cu_{240} is by far the most energetically favourable one; the small sizes of its component have the time to rearrange into a highly ordered structures by the end of the simulations.

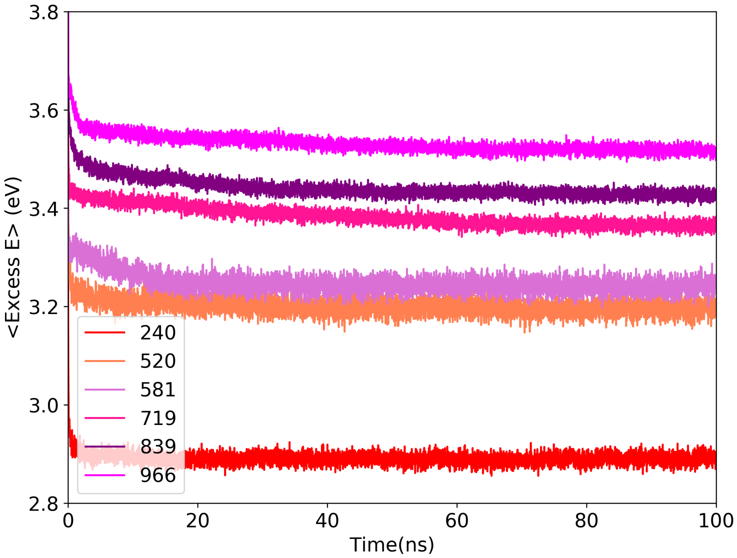

Figure 4: Excess energy evolution in coalescence processes. The results are averaged over the 10 independent runs for each size. The legend represents the number of atoms, namely the size of the NP.

If the final structures for each process are taken into account, it is found that frozen, ordered structures resulting from a freezing (if brought to 200 K) are the most energetically favourable ones, followed by the grown ones, and finally, by the collided ones.

VI. NEAS evolution

Figure 5 shows example evolutions of the aGCN distributions in representative trajectories for nanoparticles of different sizes, undergoing one of the three formation processes under consideration.

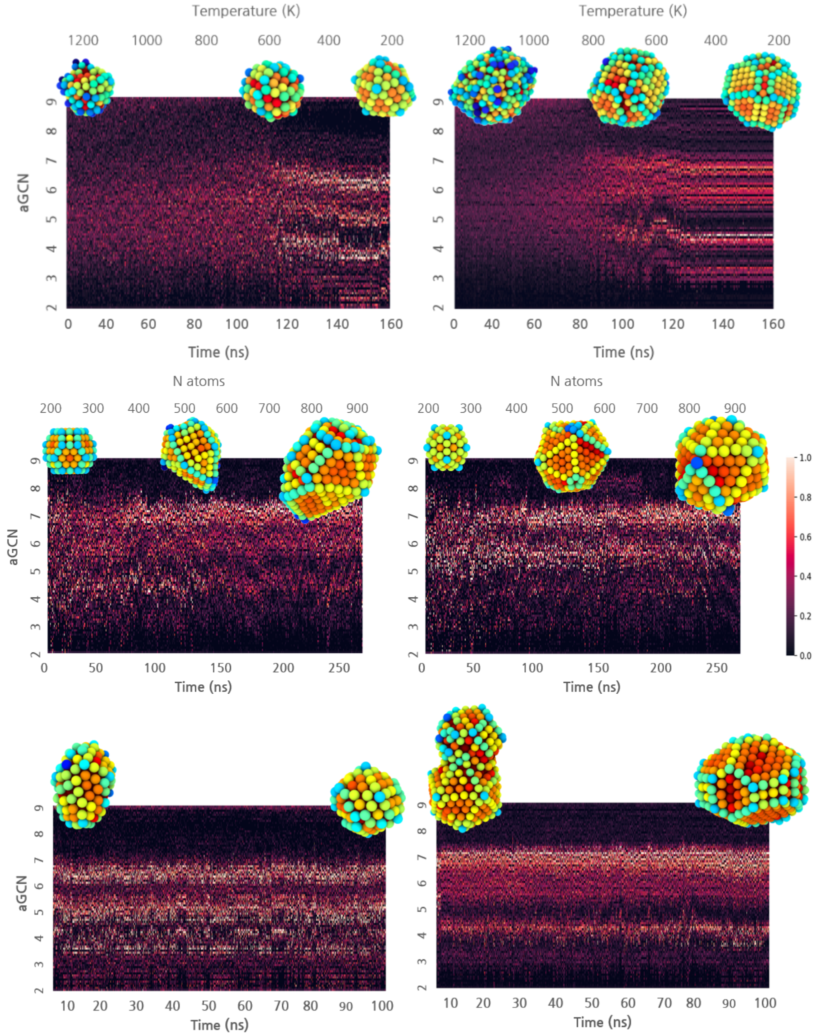

Figure 5: Evolution of the aGCN genome occurrence. Snapshots at specific times (time evolution going left to right) are taken for *i)* a freezing of Cu$_{250}$, *ii)* a freezing of Cu$_{976}$, *iii)* a growth from Cu$_{201}$(FCC) to Cu$_{997}$, *iv)* a growth from Cu$_{147}$ (Ih) to Cu$_{997}$,*v)* a coalescence of Cu$_{110}$+Cu$_{130}$ and *vi)* a coalescence of Cu$_{434}$+Cu$_{285}$. Atoms are colored according to their aGCN following the color palette of Figures 2 and 4 of the main text, to show that aGCN values between 2 and 9 belong to the NPs' surfaces.

VI. 100 ns Equilibrated structures

The observation time we adopted for annealed and atom-by-atom grown structures, together with the height of the barriers around the local minima we visit, determine the portion of the free energy landscape one can sample.

We thus consider 100 ns of equilibration for example isomers sampled during atom-by-atom growth or at the end of an annealing process.

By monitoring the excess energy of each system over time, Figure 6 we do not observe any signature of significant solid-solid rearrangements.

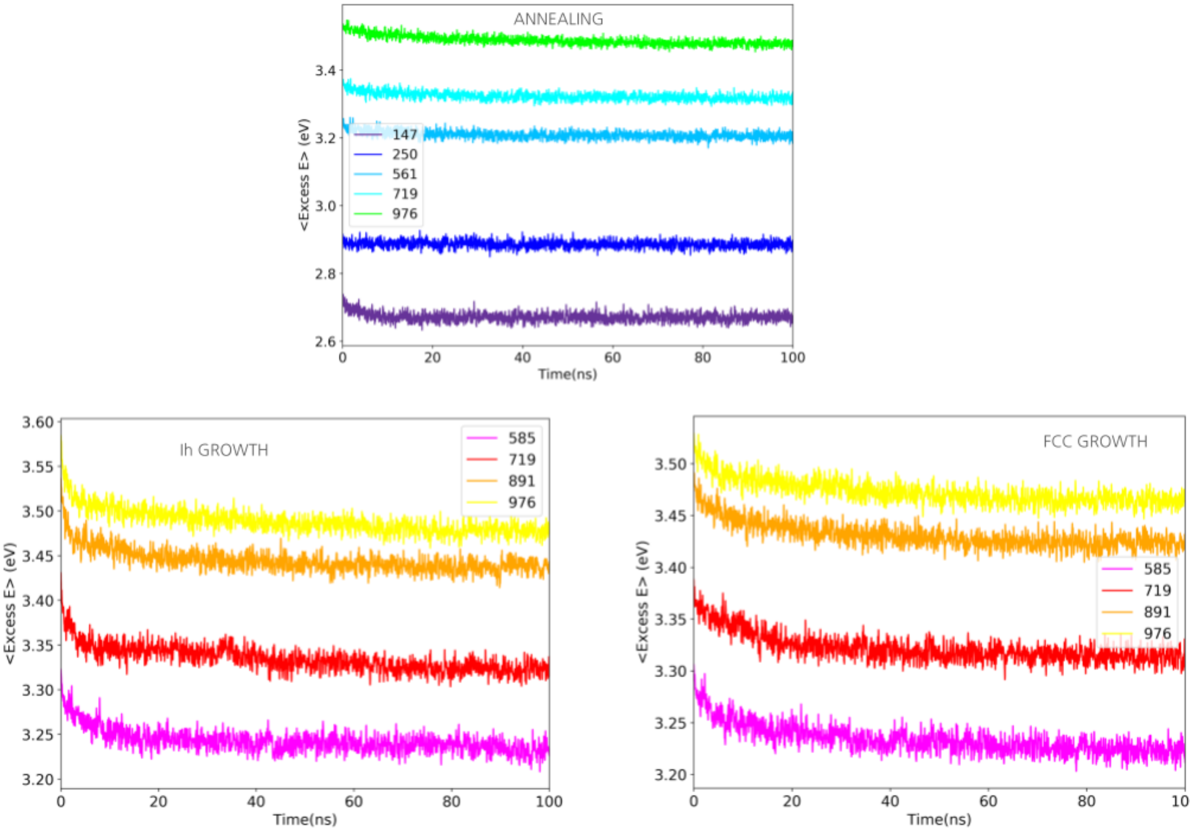

Figure 6: Average NEAS distribution for an ensemble of 10 structures sampled at the end of a 100 ns.

This is also confirmed by looking at the evolution over time for the aGCN NEAS distributions. The latter display only small oscillations, as shown for paradigmatic cases in Figure 7. The figure reports on Cu561 (top) and Cu719 (bottom) nanoparticles whose starting morphology was found sampled at the end of the annealing of a liquid droplet.

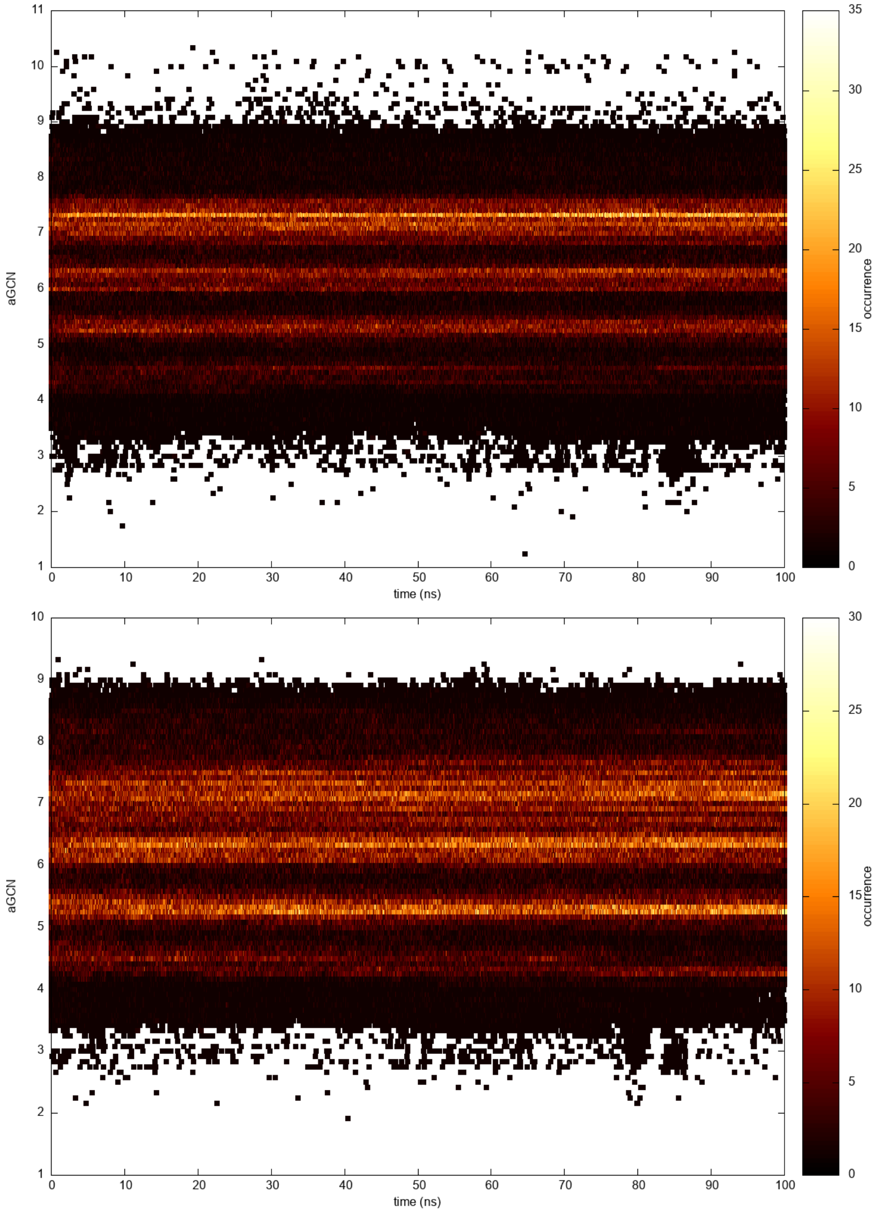

Figure 7: Time evolution of the aGCN occurrences in a Cu561 (upper panel) and Cu719 (lower panel) during a NVT run 100 ns.

To sum up the results of the 100 ns NVT runs, we report in Figure 8 the NEAS distributions observed in ensembles of structures found at the end of annealing or atom-by-atom growth processes.

The NEAS distributions differences among nanoparticles of different sizes and found during different formation processes are confirmed also for sampling utilising a longer observation timescale.

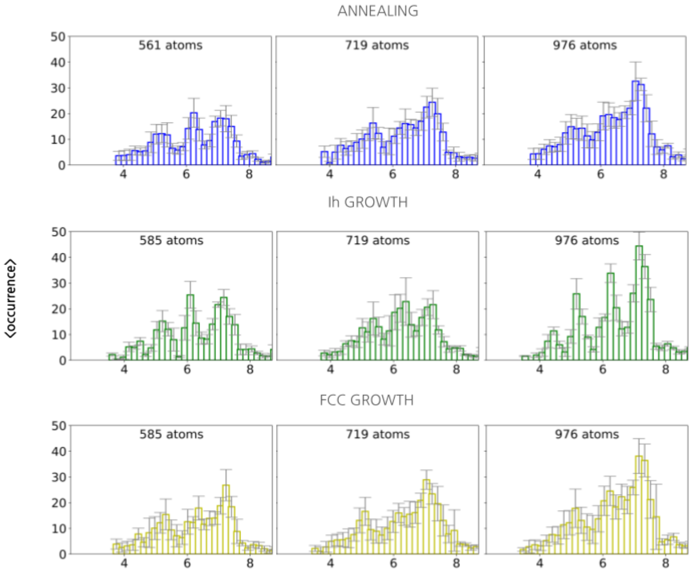

Figure 8: Average NEAS distribution for an ensemble of 10 structures sampled at the end of a 100 ns.

VII. Bootstrapping analysis for NEAS distributions and predicted activity

We look at 6 blocks of 5 independent runs randomly extracted from our 10 simulations and observe that the observable statistics, i.e. the predicted MAs, do not change significantly even if we choose a reduced number of simulations. As observed in Figure 9, from a quantitative perspective the predicted MAs may vary by few (mA/mg). Nevertheless, the size-activity trends we observed are always confirmed from a qualitative standpoint.

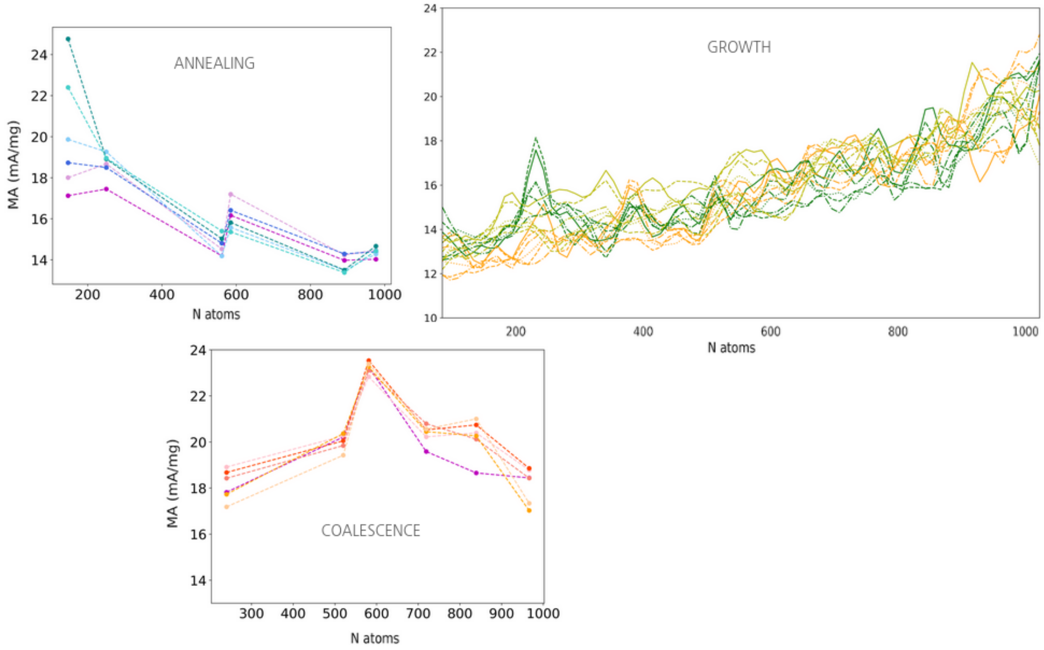

Figure 9: Mass activity trends for 6 sets of 5 randomly selected runs extracted from the 10 simulations we performed for annealing, atom-by-atom-growth, and coalescence simulation.

IX. Cut-off sensitivity analysis, NEAS distribution, and predicted activity

We perform a sensitivity analysis to probe the effect of the choice of the first nearest neighbours cut-off radius (r_{cut}) on the predicted MA. While in the main text we report data found for $r_{cut} = 3.145$Åwe here probe the 2.63-3.63Årange. The results of this analysis are reported in Figure 10, 11, and 12. The trends reported in the main manuscript are qualitatively, if not quantitatively, confirmed for any cut-off choice in the 3-3.6nm range.

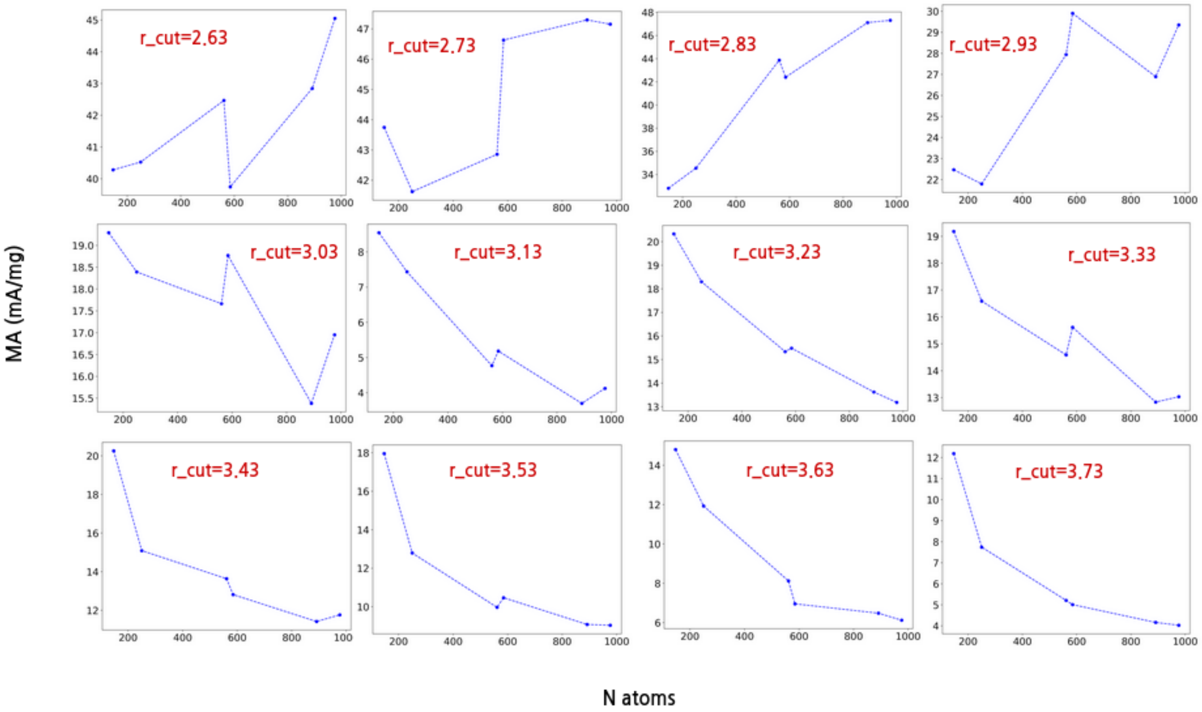

Figure 10: MA prediction as a function of NP size and r_{cut} choice (see legend) for NPs sampled at the end of an annealing process. r_{cut} unit is Å.

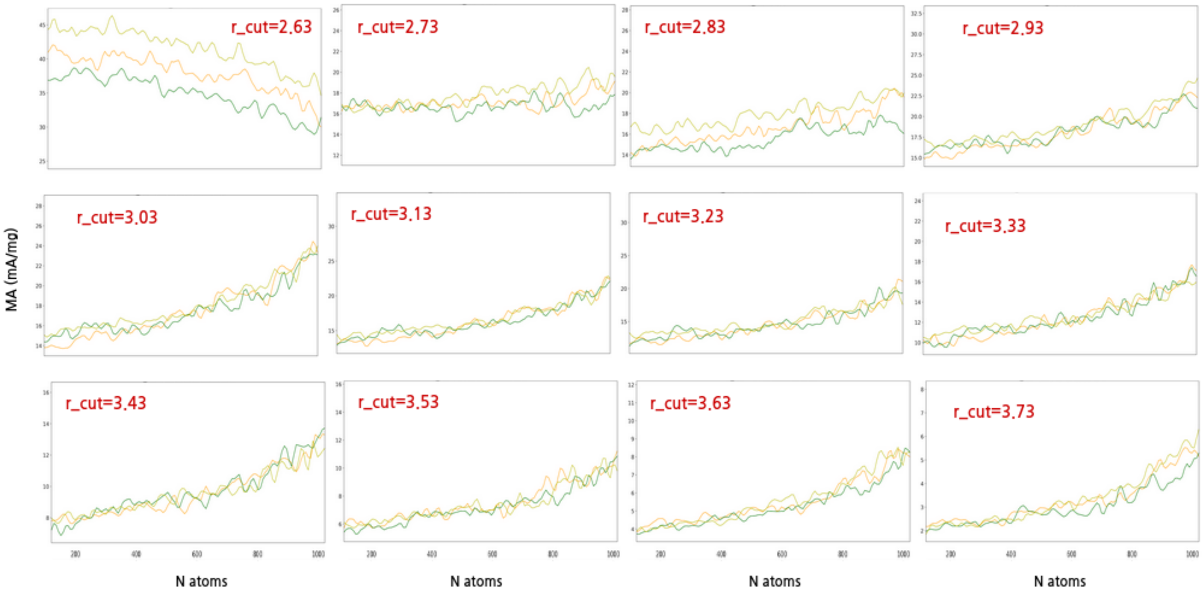

Figure 11: MA prediction as a function of NP size and r_{cut} choice (see legend) for NPs sampled during an atom-by-atom growth process. r_{cut} unit is Å.

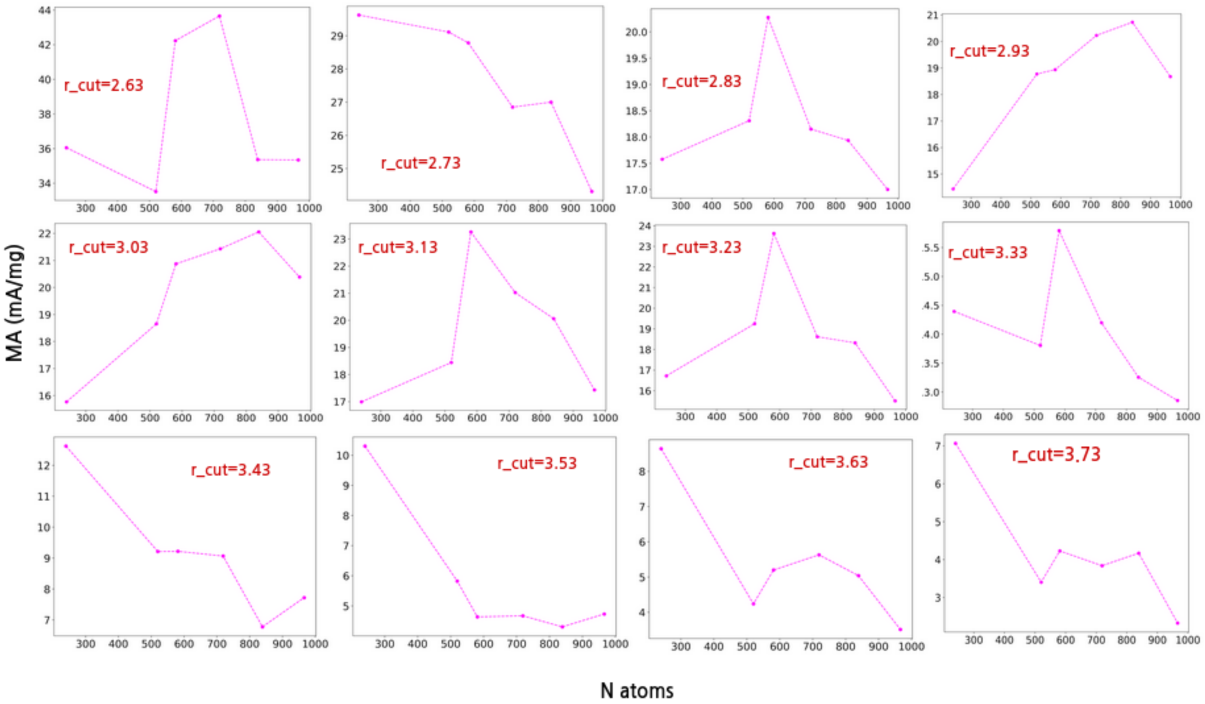

Figure 12: MA prediction as a function of NP size and r_{cut} choice (see legend) for NPs sampled at the end of a coalescence formation.r_{cut} unit is Å.

Interestingly for smaller cut-off choices, closer to the putative bulk nearest neighbour distance, we observe different trends and larger MA magnitudes, which we also reported for reference. Nevertheless we strongly believe that the choice of any cutoff radius below 3A is going to severely underestimate the NEAS coordination. To rationalize this argument we refer the interested read to Figure 13. The latter shows the distribution of atom-atom distances averaged over the full set of snapshots (1 every 10 ps) sampled in paradigmatic trajectories. The first neighbour peak is centered at the expected first nearest neighbour distance (2.67 Å= 3.61 Å× 0.707). However metallic bond distances are distributed so that also shortened as well as elongated ones appear. This motivates our choice of taking a cut-off which is in between the bulk first and second nearest neighbour distances, i.e. 3.145Å.

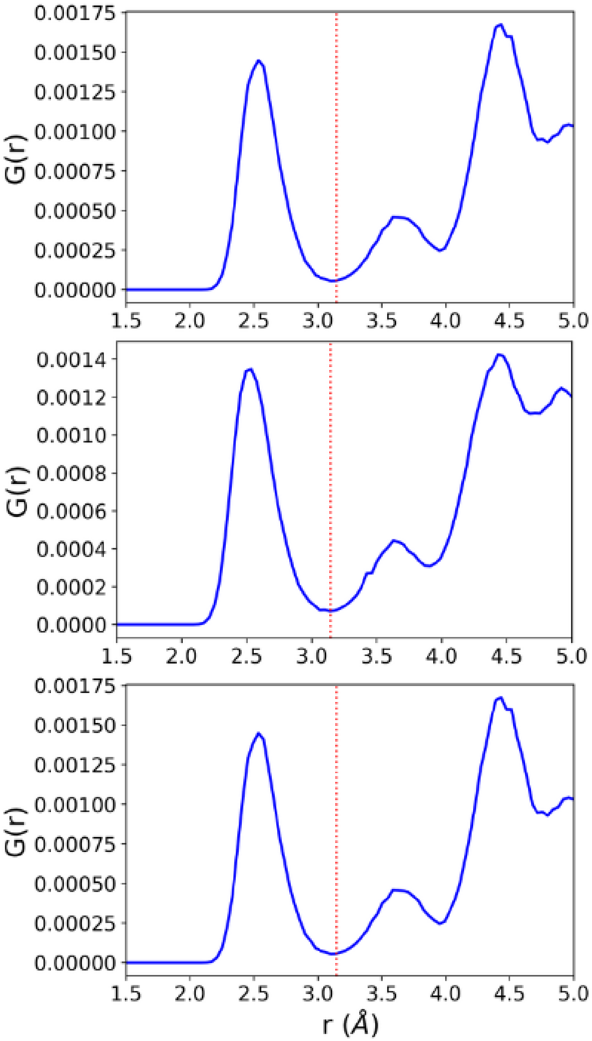

Figure 13: Example averaged PDF for i)annealing of Cu_{585} ii) growth from an Ih_{147} and iii) coalescence for Cu_{581}. PDF are normalized so that the sum of each bin (0.005 Å) is equal to one. Splines fitting is used to smooth the result.

References

(1) Baletto, F.; Ferrando, R. Structural properties of nanoclusters: Energetic, thermodynamic, and kinetic effects. *Rev. Mod. Phys.* **2005**, *77*, 371–423.

(2) Frenkel, D.; Smit, B.; Tobochnik, J.; McKay, S.; Christian, W. Understanding Molecular Simulation. *Computers in Physics* **1997**, *11*, 351.

(3) https://github.com/orgs/kcl tscm/teams/lodis, LoDiS - a low dimensional systems molecular dynamics engine. **2019**,

(4) Rossi, K.; Bartok-Partay, L.; Csányi, G.; Baletto, F. Thermodynamics of CuPt nanoalloys. *Scientific Reports* **2018**, *8*.

(5) Honeycutt, J.; Andersen, H. Molecular-Dynamics Study of Melting and Freezing of Small Lennard-Jones Clusters. *The Journal of Physical Chemistry* **1987**, *91*, 4950–4963.

(6) Nørskov, J.; Rossmeisl, J.; Logadottir, A.; Lindqvist, L.; Kitchin, J.; Bligaard, T.; Jonsson, H. Origin of the Overpotential for Oxygen Reduction at a Fuel-Cell Cathode. *Journal of Physical Chemistry B* **2004**, *108*, 17886–17892.

(7) Hori, Y.; Takahashi, R.; Yoshinami, Y.; Murata, A. Electrochemical Reduction of CO at a Copper Electrode. *Journal of Physical Chemistry B* **1997**, *101*, 7075–7081.

(8) Zhao, Z.; Chen, Z.; Zhang, X.; Lu, G. Generalized Surface Coordination Number as an Activity Descriptor for CO 2 Reduction on Cu Surfaces. *The Journal of Physical Chemistry C* **2016**, *120*, 28125–28130.

(9) Loiudice, A.; Lobaccaro, P.; Kamali, E.; Thao, T.; Huang, B.; Ager, J.; Buonsanti, R. Tailoring Copper Nanocrystals towards C2 Products in Electrochemical CO2 Reduction. *Angewandte Chemie (International ed. in English)* **2016**, *128*, 5789–5792.

(10) Kevin, R. Multiscale modelling of metallic nanoparticles structural and catalytic properties. *KCL PhD Thesis* **2019**,

References

(1) Baletto, F.; Ferrando, R. Structural properties of nanoclusters: Energetic, thermodynamic, and kinetic effects. *Rev. Mod. Phys.* **2005**, *77*, 371–423.

(2) Frenkel, D.; Smit, B.; Tobochnik, J.; McKay, S.; Christian, W. Understanding Molecular Simulation. *Computers in Physics* **1997**, *11*, 351.

(3) https://github.com/orgs/kcl tscm/teams/lodis, LoDiS - a low dimensional systems molecular dynamics engine. **2019**,

(4) Rossi, K.; Bartok-Partay, L.; Csányi, G.; Baletto, F. Thermodynamics of CuPt nanoalloys. *Scientific Reports* **2018**, *8*.

(5) Honeycutt, J.; Andersen, H. Molecular-Dynamics Study of Melting and Freezing of Small Lennard-Jones Clusters. *The Journal of Physical Chemistry* **1987**, *91*, 4950–4963.

(6) Nørskov, J.; Rossmeisl, J.; Logadottir, A.; Lindqvist, L.; Kitchin, J.; Bligaard, T.; Jonsson, H. Origin of the Overpotential for Oxygen Reduction at a Fuel-Cell Cathode. *Journal of Physical Chemistry B* **2004**, *108*, 17886–17892.

(7) Hori, Y.; Takahashi, R.; Yoshinami, Y.; Murata, A. Electrochemical Reduction of CO at a Copper Electrode. *Journal of Physical Chemistry B* **1997**, *101*, 7075–7081.

(8) Zhao, Z.; Chen, Z.; Zhang, X.; Lu, G. Generalized Surface Coordination Number as an Activity Descriptor for CO 2 Reduction on Cu Surfaces. *The Journal of Physical Chemistry C* **2016**, *120*, 28125–28130.

(9) Loiudice, A.; Lobaccaro, P.; Kamali, E.; Thao, T.; Huang, B.; Ager, J.; Buonsanti, R. Tailoring Copper Nanocrystals towards C2 Products in Electrochemical CO2 Reduction. *Angewandte Chemie (International ed. in English)* **2016**, *128*, 5789–5792.

(10) Kevin, R. Multiscale modelling of metallic nanoparticles structural and catalytic properties. *KCL PhD Thesis* **2019**,